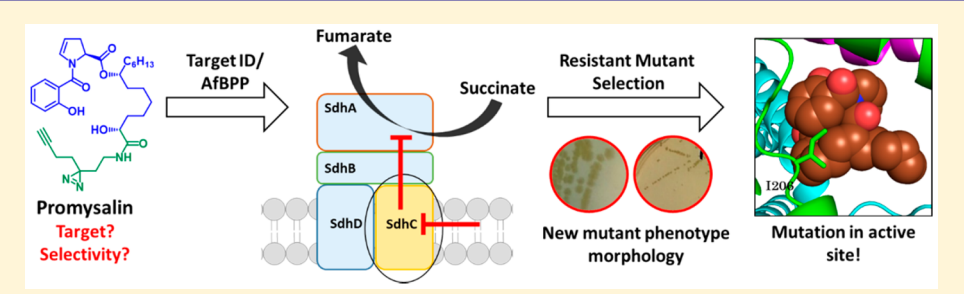


# Promysalin Elicits Species-Selective Inhibition of *Pseudomonas* aeruginosa by Targeting Succinate Dehydrogenase

Colleen E. Keohane,<sup>†</sup> Andrew D. Steele,<sup>†</sup> Christian Fetzer,<sup>‡</sup> Jittasak Khowsathit,<sup>§,○</sup> Daria Van Tyne, Lucile Moynié,<sup>#,▽</sup> Michael S. Gilmore, John Karanicolas, Stephan A. Sieber, Daria Van Tyne, Lucile Moynié, Daria Van Tyne, Daria Va and William M. Wuest\*,†

# Supporting Information



ABSTRACT: Natural products have served as an inspiration to scientists both for their complex three-dimensional architecture and exquisite biological activity. Promysalin is one such Pseudomonad secondary metabolite that exhibits narrow-spectrum antibacterial activity, originally isolated from the rhizosphere. We herein utilize affinity-based protein profiling (AfBPP) to identify succinate dehydrogenase (Sdh) as the biological target of the natural product. The target was further validated in silico, in vitro, in vivo, and through the selection, and sequencing, of a resistant mutant. Succinate dehydrogenase plays an essential role in primary metabolism of Pseudomonas aeruginosa as the only enzyme that is involved both in the tricarboxylic acid cycle (TCA) and in respiration via the electron transport chain. These findings add credence to other studies that suggest that the TCA cycle is an understudied target in the development of novel therapeutics to combat P. aeruginosa, a significant pathogen in clinical settings.

#### ■ INTRODUCTION

The continued rise of antibiotic resistant bacterial infections warrants the development of novel treatments with unique modes of action. To date, there is a general lack of diversity among cellular targets of approved antibiotics with recent reports estimating that fewer than 25 targets are represented.<sup>1</sup> Most of these compounds are nondiscriminatory (broadspectrum), and they target essential pathways such as cell wall or protein synthesis.<sup>2</sup> Although some "narrow-spectrum" therapies are available, they target large subsets of bacteria (anaerobes vs aerobes, Gram-positive vs Gram-negative) instead of focusing on particular pathogenic species. The latter method of treatment would be preferred in an effort to reduce

adverse side effects to the host and microbiome communities and to minimize the development of resistance. However, both financial and technical limitations have thwarted such efforts to date.<sup>3</sup> Furthermore, the identification of either (1) unique targets that would permit selective killing or (2) compounds that discriminate species is not trivial; this presents a clear unmet need that is ripe for discovery.

The combination of microbial diversity and evolutionary pressure has incentivized bacteria to create natural products with extraordinary selectivity and bioactivity. These scaffolds

Received: October 20, 2017 Published: January 4, 2018

<sup>&</sup>lt;sup>†</sup>Department of Chemistry, Emory University, Atlanta, Georgia 30322, United States

<sup>&</sup>lt;sup>‡</sup>Department of Chemistry, Center for Integrated Protein Science Munich (CIPSM), Technische Universität München, Lichtenbergstraße 4, 85747 Garching, Germany

<sup>§</sup>Molecular Therapeutics Program, Fox Chase Cancer Center, Philadelphia, Pennsylvania 19111, United States

Department of Ophthalmology, Harvard Medical School, Massachusetts Eye and Ear Infirmary, Boston, Massachusetts 02115, United States

<sup>&</sup>lt;sup>1</sup>Department of Microbiology and Immunobiology, Harvard Medical School, Boston, Massachusetts 02115, United States

<sup>\*</sup>Division of Structural Biology, The University of Oxford, Headington Oxford, OX3 7BN, United Kingdom

Operatment of Molecular Biosciences, University of Kansas, Lawrence, Kansas 66045, United States

Biomedical Sciences Research Complex, University of St. Andrews, Fife Scotland, KY16 9ST, United Kingdom

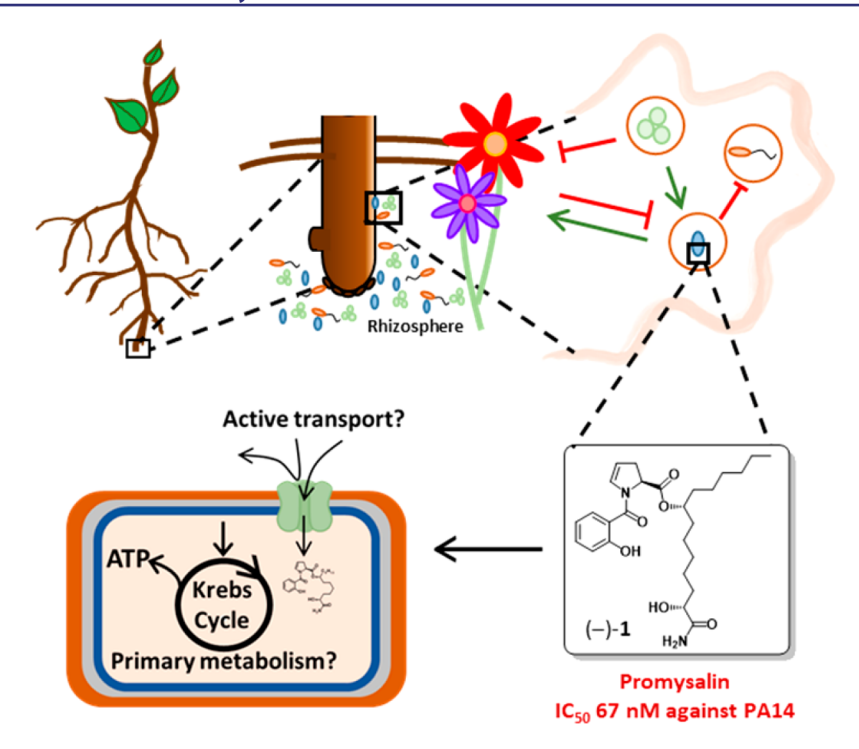


Figure 1. Schematic of the rhizosphere and the proposed mechanisms of action of promysalin.

serve with distinction as antibacterial agents as an estimated 70% of marketed antibiotics are derived from natural products. One specific example exists within the rhizosphere where predominantly Gram-negative bacteria, particularly the Pseudomonads, utilize chemical warfare to both colonize the environment (quorum sensing) and defend themselves (antibiotics).<sup>4,5</sup> Of particular health interest is the bacterial species Pseudomonas aeruginosa (Pa), an opportunistic environmental pathogen inherently resistant to many antibiotics yet rarely infective to healthy individuals.6 However, those with compromised immune systems (i.e., burn victims, chemotherapy patients, and the chronically hospitalized) or cystic fibrosis are especially susceptible to a fatal infection. In 2013, the Centers for Disease Control listed multidrug resistant Pa one of the top 15 urgent/serious microbial threats facing society, and just this year they increased its priority to the highest level, "critical", demonstrating a pressing need to develop new therapeutics which target this pathogen of interest.

Recent efforts by both the De Mot<sup>8</sup> and Muller<sup>9</sup> laboratories have focused on this call by targeting untapped resources within the soil, which are rich in diversity. Thorough work by both groups has revealed natural products with complex chemical architecture and unique bioactivity providing inspiration for organic chemists as platforms for further discovery. One such example is the Pseudomonad secondary metabolite promysalin, which possesses species-selective inhibitory activity against Pa (initially reported IC<sub>50</sub> = 0.83  $\mu$ g/mL; MBC = 100  $\mu$ g/mL against PA14), while inducing swarming and biofilm formation in a related species, P. putida (Pp). In 2015, our group completed the first total synthesis of the natural product, which enabled our elucidation of promysalin's relative and absolute stereochemistry and also confirmed the reported biological activity. 11 We also showed for the first time that promysalin repressed fluorescence of P. putida KT2440, which is presumably attributed to the inhibition of pyoverdine

production by the bacterium. We postulated that this phenotype might result from its ability to bind iron and therefore synthesized a concise library of analogs to test this hypothesis. Not only did this work provide initial structure—activity relationships that guided the findings provided herein, but it also confirmed that promysalin was capable of chelating iron, albeit weakly.

Despite the interesting and unique biological effects of promysalin, its mode of action remained unclear. Two potential mechanisms could explain the species-selective mode of action of this natural product. First, promysalin might act as a sideromycin, an antibiotic that hijacks siderophore transport through an iron-binding motif (Figure 1). Alternatively, promysalin could be targeting a difference in primary metabolism between species of *Pseudomonads*. The latter mechanism initially seemed counterintuitive: one would not expect that an essential enzyme, critical to nearly all life, could be the target of a narrow-spectrum agent. Nonetheless, here we report the surprising finding that the target of promysalin is succinate dehydrogenase (Sdh), a conserved enzyme that plays a key role in both in the tricarboxylic acid cycle (TCA) and in respiration.

# **■ RESULTS**

The Inhibitory Activity of Promysalin Is Not Affected by Iron Concentration. Previous reports have demonstrated that the inhibitory activity of sideromycins is correlated to iron concentration as they rely on a chelation strategy to penetrate bacterial cells. <sup>14</sup> In an elegant display of chemical creativity, the Miller group used these molecules as inspiration and developed a second-generation of synthetic sideromycins, whereby established antibiotics were covalently tethered to known siderophores, effectively creating a "Trojan Horse" strategy that was remarkably successful. <sup>15,16</sup> This approach is best exemplified by BAL30072, a novel siderophore-sulfactam conjugate that entered Phase 1 clinical trials. <sup>17</sup> Similarly,

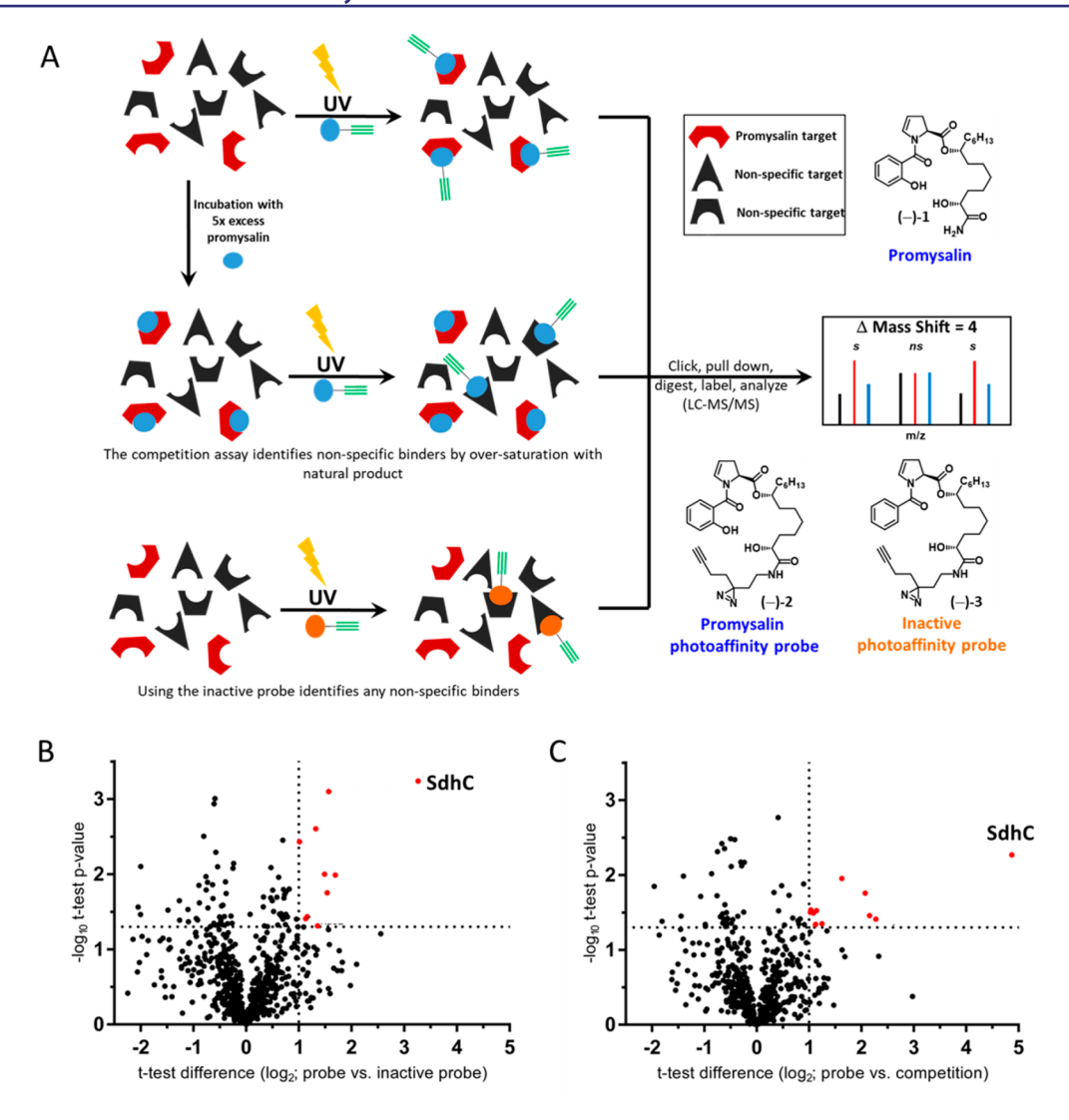


Figure 2. (A) General AfBPP workflow. Bacteria are incubated with promysalin probe, (-)-2 (top), promysalin ((-)-1) *then* promysalin probe (middle), or inactive probe, (-)-3 (bottom), and then irradiated. Biotin-azide click chemistry permits pull down and subsequent digestion and labeling allows for the identification of enriched proteins. Volcano plots of significantly enriched proteins in PA14 compare the difference in selectivity with either an inactive probe (B) or competitive inhibitor (C). Concentrations of 3  $\mu$ M were used for both the probe and inactive probe and 30  $\mu$ M for the natural product in competition experiments.

these molecules also rely on iron concentration and their activity can be enhanced by either the introduction of strong iron chelators or prior removal of iron from the media. Based on this knowledge, we sought to probe the bioactivity of promysalin against Pa strains PAO1 and PA14 over a range of iron concentrations. Under iron-limited conditions, we expected transcriptional upregulation of iron transport systems would facilitate the diffusion of promysalin into the cell and consequently increase its potency akin to sideromycins. However, our studies revealed that there was no identifiable effect of the available iron on efficacy as indicated by  $IC_{50}$  values, suggesting that iron chelation is coincidental and separate from antibiotic activity.

Previous work investigating the mechanism of action of BAL30072 identified the iron receptor PiuA as the active transporter responsible for the uptake of the molecule into Pa. PiuA is a member of the TonB dependent transporter (TBT) family, which are membrane-bound proteins responsible for the active transport of siderophores by means of the proton motive force. Transcription of such systems is up-regulated in

response to stress<sup>20</sup> and conversely down-regulated when an equilibrium is met, as excess iron is toxic. Previous findings have shown that TBTs regulate pyoverdine production and also vary widely between Pseudomonads, which could potentially explain our prior results. Initially, we investigated the ability of promysalin to form an Fe3+-bound complex with a variety of iron sources (Fe(acac)<sub>3</sub>, (NH<sub>4</sub>)<sub>5</sub>[Fe(C<sub>6</sub>H<sub>4</sub>O<sub>7</sub>)<sub>2</sub>], and FeCl<sub>3</sub>) by UV-visible spectroscopy. In all instances, we did not observe the characteristic Fe<sup>3+</sup>-siderophore complex at ~500 nm seen in other systems like enterobactin (Figure S1). Recently, one of our laboratories solved the crystal structure of PiuA and revealed the putative binding site of BAL30072.<sup>19</sup> To further confirm that promysalin was not interacting via the PiuA system we sought to use isothermal microcalorimetry titration experiments to determine the extent at which the natural product binds. However, these studies again refuted our earlier hypothesis as no appreciable interaction was observed (Figure S2). Taken in sum, these findings demonstrate that although promysalin is capable of binding iron, it does not appear to be

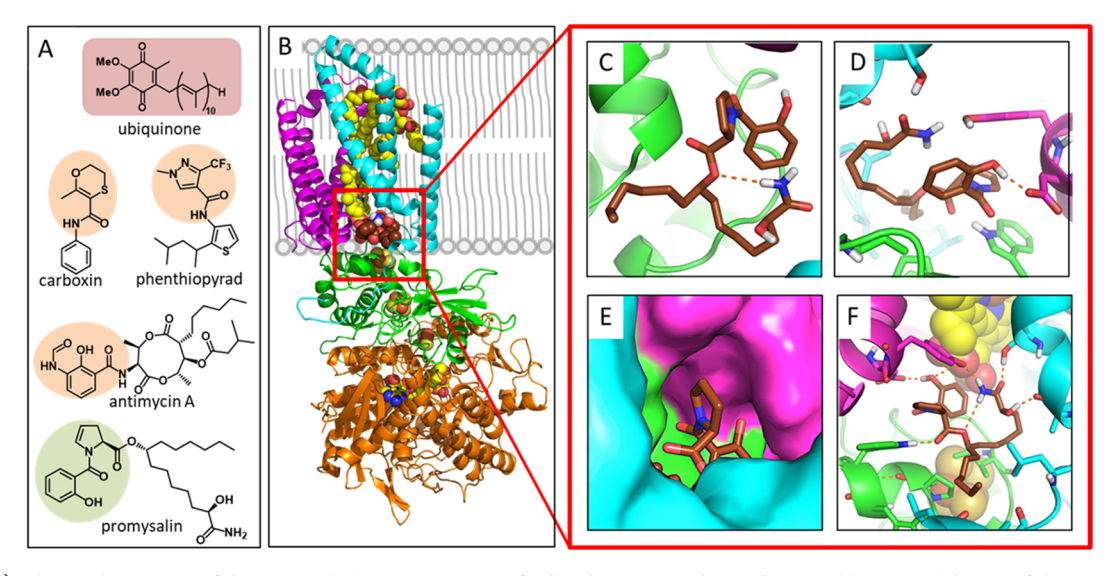


Figure 3. (A) Chemical structure of the terminal electron acceptor of Sdh, ubiquinone, alongside several known inhibitors of the complex that also engage the ubiquinone-binding site. Moieties that exhibit similarity to promysalin are highlighted. (B) Model of *P. aeruginosa* Sdh was built from the closely related *E. coli* structure. Promysalin (brown) is shown at the ubiquinone-binding site using our modeled binding mode. The subunits of SdhA, SdhB, SdhC, and SdhD are colored orange, green, cyan, and pink, respectively. Redox centers involved in the electron transport pathway are shown in yellow. (C) The model of promysalin binding includes an intramolecular hydrogen bond between the amide tail and the ester linker, consistent with previous SAR pointing to the importance of this ester. (D) The model includes an intermolecular hydrogen bond involving the salicylate hydroxyl group, further consistent with previous SAR. (E) The dehydroproline ring faces outward in the model, again consistent with previous SAR. (F) The model of promysalin binding includes interactions with all three subunits that surround the ubiquinone-binding site, and explains additional experimental observations that were not used in developing the model.

acting as a viable siderophore and/or using siderophore transport channels to elicit its response.

Affinity-Based Protein Profiling Identifies Succinate Dehydrogenase as the Biological Target of Promysalin. With our initial siderophore-based hypothesis disproven, we next planned to implement affinity-based protein profiling (AfBPP) to identify likely candidates. At the onset of this project, it was unclear if promysalin covalently modified its target; we therefore decided to install a photoaffinity probe to ensure capture of the biological moiety. The Yao group previously developed a concise route to a stand-alone diazirine photoprobe flanked on one end with an alkyne for AfBPP and a primary amine on the other primed for amidation chemistry.<sup>2</sup> Initially, we envisioned installing the diazirine photoprobe to the side chain hydroxyl group, as that position was reactive based on our protecting group scheme from our previous total synthesis; however, our previous analog studies discouraged this modification.<sup>22</sup> Instead, we focused our efforts on the alkylation of the amide nitrogen, which can be easily accessed from our earlier routes. For preliminary screening, we appended a propargyl moiety to the amide nitrogen, S4, (Scheme S1), which was approximately 3-fold less active than the natural product (218 vs 67 nM in PA14), thus permitting our strategy to synthesize the amide probe (full synthetic details are provided in the Supporting Information). Antibacterial activity of the probe was confirmed, with an IC50 value of 1.7  $\mu$ M (in PA14), supporting its use for proteomic studies.

With the probe in hand we turned to AfBPP to elucidate the protein targets of promysalin. For each experiment, three different sample types were prepared for gel-free in situ proteomic analysis (Figure 2A). Cultures of *P. aeruginosa* PAO1 and PA14 were grown to log phase and incubated with either (1) promysalin photoprobe, (-)-2, (2) inactive promysalin photoprobe, (-)-3, or (3) promysalin (-)-1 followed by promysalin photoprobe (-)-2 (competitive inhibitor); experi-

ments (2) and (3) serve to identify and eliminate any false positives. After UV irradiation, cells were lysed, reacted in situ with biotin-azide, and enriched on avidin beads. Enriched proteins were subjected to a trypsin-digest and labeled with light, medium or heavy isotopes via dimethyl-isotope labeling. Isotope labels were switched throughout biological replicates and samples with corresponding labels were pooled prior to LC-MS/MS measurement. Statistical analysis revealed only a small number of significantly (p-value  $\leq$ 0.05;  $\log_2$ -ratio  $\geq$ 1) enriched proteins (Figures 2B,C and S3). The most prominent hit in both Pa strains (PAO1 and PA14) as visualized by the volcano plot in Figure 2 was the succinate dehydrogenase C-subunit (SdhC); furthermore, the enrichment could be outcompeted by promysalin thereby providing preliminary validation of SdhC as the biological target.

In efforts to initially confirm our proteomic studies we sought to determine an in vitro IC<sub>50</sub> against Sdh itself. While previous reports mention isolating Sdh from Pa membranes we instead leveraged a commercially available colorimetric mitochondrial Sdh assay. This would both give us confidence in Sdh as the target (as bacterial and mammalian enzymes are homologous) and provide information regarding selectivity between the two kingdoms. We observe complete inhibition of complex II at 200  $\mu$ M and an IC<sub>50</sub> of 2.5  $\mu$ M. It should be noted that the ~50-fold difference in activity between the in vitro mammalian assay and the in vivo bacterial studies suggests that promysalin preferentially targets bacteria, which warrants future studies.

Computational Molecular Docking Supports Succinate Dehydrogenase as the Target of Promysalin. With consistent proteomic data and in vitro inhibitory activity in hand we sought to identify a putative binding site with computational modeling. Ideally, we would have preferred to cocrystallize promysalin with Sdh; however, the *Pseudomonas* protein has not yet been crystallized. The homologous enzyme

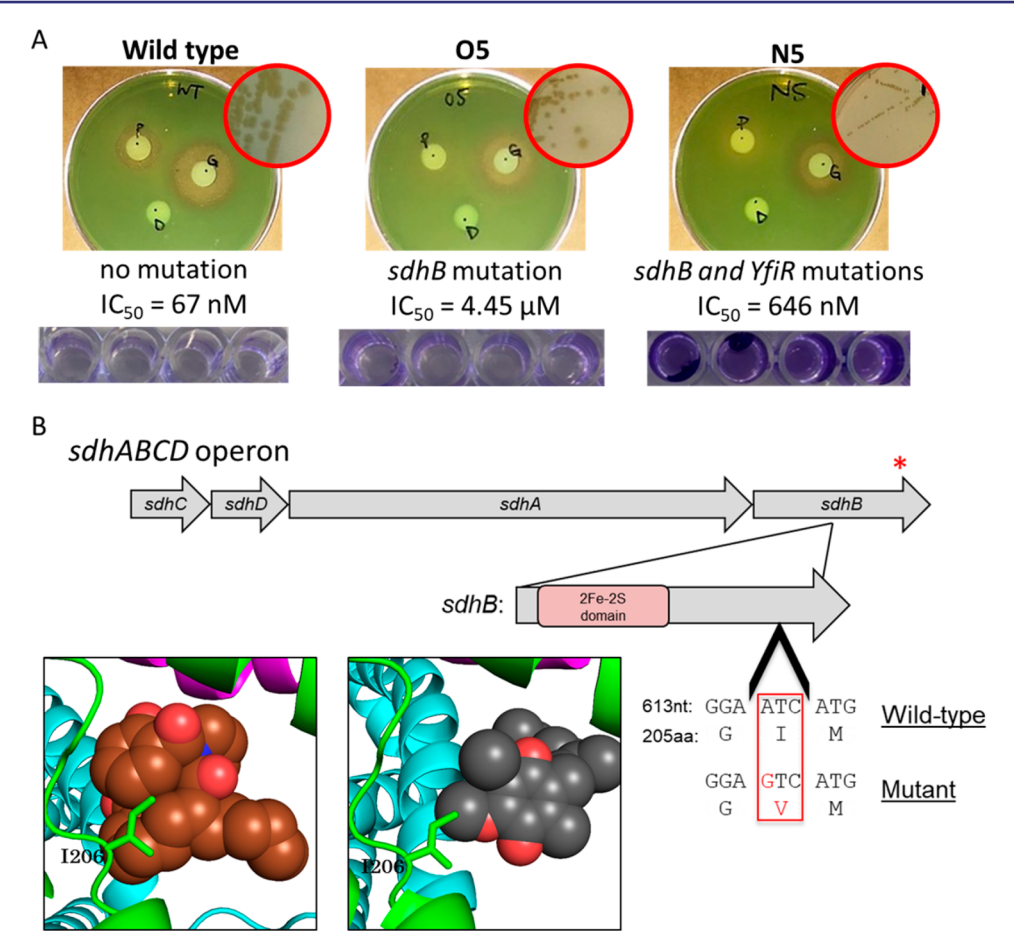


Figure 4. (A) Zone of inhibition for PA14 wild type (left) and both mutants O5 (middle) and N5 (right) when treated with promysalin (P), gentamicin (G), and DMSO (D). Insets show different morphologies (SCV on right). Below is crystal violet staining of untreated cells depicting the increase in biofilm formation for strain N5. (B) Location of the I206V mutation associated with promysalin resistance. Below, the *sdhB* gene is depicted, including the 2Fe-2S iron—sulfur cluster binding domain and showing the single-nucleotide polymorphism and amino acid change associated with promysalin resistance. At bottom, the structure of the binding pocket is shown with promysalin (left) and ubiquinone (right), highlighting the location of I206.

in *E. coli* has been structurally characterized,<sup>25</sup> and thus this served as a starting point for modeling the *Pseudomonas* enzyme. Previous work also identified several small molecules that inhibit *E. coli* Sdh at the ubiquinone-binding site (Figure 3A), and based on shared structural features of these compounds we anticipated that promysalin would bind at the analogous site (Figure 3B).<sup>26</sup>

We aligned each of these known inhibitors onto the *Pseudomonas* enzyme then used these compounds as the basis for pharmacophoric matching using a broad range of possible promysalin three-dimensional conformations. Upon energy minimization, these yielded many bound poses with comparable predicted energetics; thus, we leveraged our existing structure—activity relationship (SAR) data to narrow down the possible models.<sup>22</sup>

To our satisfaction, we found that the SAR was fully consistent with only *one* of these very diverse models: this points to the stringency of the constraints that arise from our thorough SAR characterization and provides confidence in the final model. There are three key observations that allowed us to reject all possible models but this one. First, we previously reported that the replacement of the ester linker with an amide abolished activity: in the docked model the ester adopts a conformation where the oxygen is engaged in intramolecular hydrogen bonding, whereas an amide substitution here would

abolish this favorable interaction (Figure 3C). Second, replacing the salicylate hydroxyl group with a methoxy group greatly reduced activity: in the docked model this hydroxyl group engages in hydrogen bonding with a nearby aspartate and tyrosine; alkylating the oxygen would render these interactions impossible (Figure 3D and F). Finally, adding a methyl group to the dehydroproline heterocycle resulted in a compound with moderate activity; in the docked model this position points outward from the binding pocket, explaining how incorporation of an extra substituent is tolerated (Figure 3F)

This model is additionally consistent with information that was not part of the SAR used in its selection (Figure 3F). The model includes a hydrogen bond between a backbone carbonyl of SdhC and the alcohol side chain on the myristate region: the modeled position and orientation of the side chain alcohol explains why its stereochemistry was important for activity (changing this stereochemistry would lead to a steric clash), and yet its removal was also tolerated. Separately, we note that promysalin must bind in a manner that can accommodate the diazirine photoprobe with only minimal effects on bioactivity (~10× less active): the terminal amide in this model engages in two hydrogen bonds with the enzyme, and still would allow the alkyne moiety of the photoprobe to project toward the hydrophobic groove occupied by the fatty acid side chain.

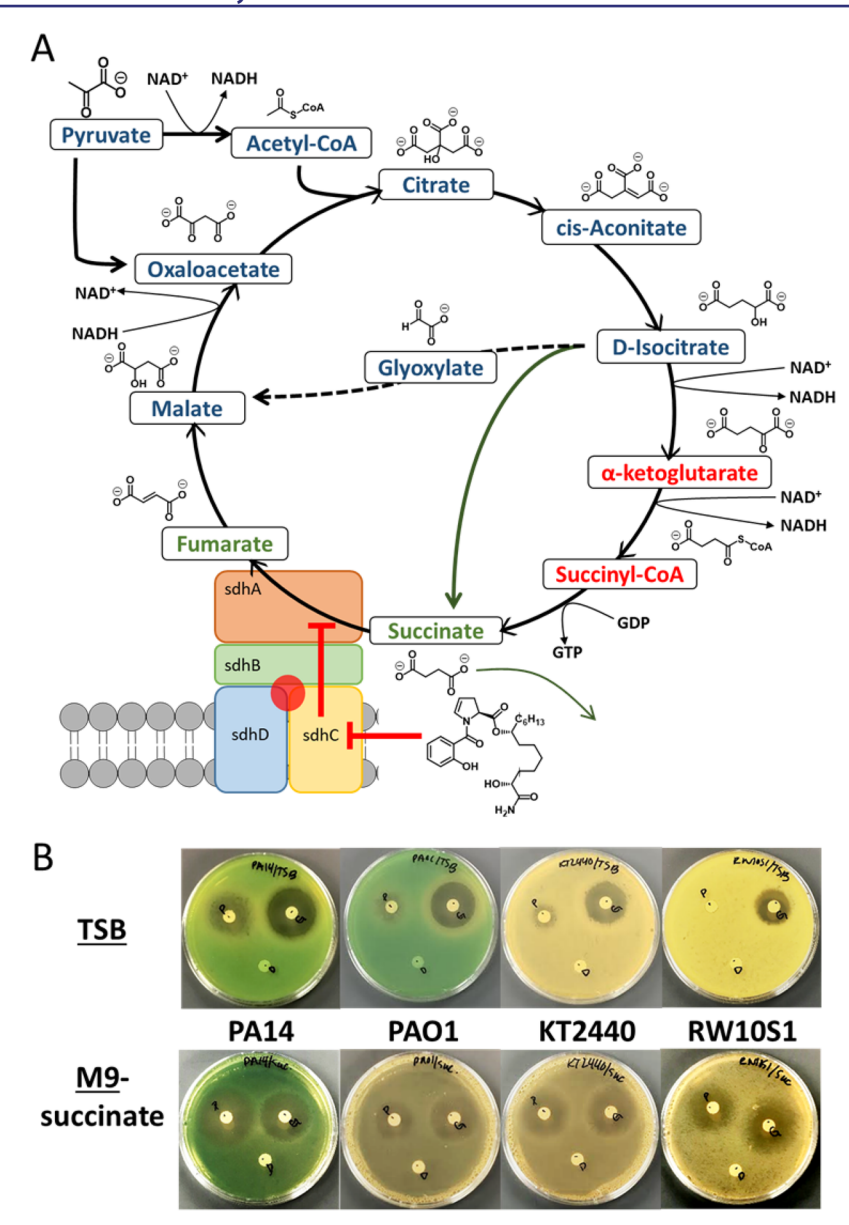


Figure 5. (A) Representation of the TCA cycle and glyoxylate shunt pathway. Promysalin inhibits Sdh, which in turn inhibits the TCA pathway (bottom left). (B) Zone of inhibition assay in TSB (nutrient rich media, top) and M9 minimal media (with succinate as sole carbon source, bottom) against PA14, PAO1, PP KT2440, and PP RW10S1 (producing strain), L to R, when treated with promysalin (P), gentamicin (G), and DMSO (D).

Another key consequence of this model relates to the strainspecific activity of promysalin. We mapped the sequences for each Sdh subunit for PAO1, PA14, and KT2440 back onto this model of binding: notably, there was not a single sequence difference among the three at this site. The model therefore implies that the observed differential activity is not based on binding preferences of promysalin for Sdh, but rather upon some other factor that distinguishes these strains.

Whole Genome Sequencing of Promysalin-Resistant PA14 Identifies a Mutation in Succinate Dehydrogenase. There is precedence that bacteria and fungi can generate resistance to Sdh inhibitors. For example, carboxin resistance is of major concern in the agriculture industry and a number of Sdh mutations have been disclosed which render the compound inactive. <sup>27,28</sup> In an effort to validate both our proteomic results and our proposed docking model we sought to select for a promysalin-resistant mutant in PA14. Toward this end, bacteria were subjected to a range of concentrations

(sub-lethal to lethal) of promysalin daily for a 24-day period. After the course of treatment, two morphologically distinct mutant strains were obtained (Figure 4A). Strain O5, which had a similar morphology to that of the parent strain was >60-fold more resistant to promysalin. The mutant contained a nonsynonymous single nucleotide polymorphism (SNP) in SdhB, which resulted in an I206V mutation within the ubiquinone binding site at the interface of SdhB and SdhC (Figure 4B). This subtle mutation is unique to promysalin as it has not been identified in carboxin-resistant strains and is likely attributed to a greater loss of hydrophobic contact with promysalin when compared to ubiquinone.

A second resistant strain (N5) was also identified and based on its "abnormal" morphology was suspected of having distinct mutations. Whole genome sequencing (WGS) of this strain revealed the same SNP in Sdh and a second mutation in YfiR, a regulator of intracellular c-di-GMP levels.<sup>29,30</sup> YfiR mutants have been shown to form small colony variants (SCVs) thereby

explaining the altered morphology.<sup>30</sup> SCVs due to YfiR mutation, which were initially isolated from the lung of a cystic fibrosis patient, are known to possess higher levels of persistence and biofilm formation. 30 Strain N5 displayed a 10fold increase in resistance to promysalin ( $IC_{50} = 646 \text{ nM}$ ) and a significant increase in biofilm formation, in line with previous studies of this mutation (Figure 4A). Taken in sum, the WGS data further validates our proteomic, in vitro, and docking model confirming succinate dehydrogenase as the biological target of promysalin in PA14.

Promysalin Leverages Differences in the Metabolic Flux of the Tricarboxylic Acid Cycle To Elicit Species-Selectivity. The tricarboxylic acid (TCA) cycle is an essential pathway in primary metabolism and facilitates the release of stored energy through a series of eight reactions.<sup>31</sup> Succinate dehydrogenase is an enzyme that is part of both the TCA cycle and the electron transport chain (housed in membrane).<sup>32</sup> Its specific function within the process is to catalyze the oxidation of succinate to fumarate with simultaneous reduction of the cofactor ubiquinone (CoQ<sub>10</sub>) to ubiquinol (Figure 5A). Under stress, however, alternative pathways can be employed. The glyoxylate shunt pathway is one such alternative which circumvents four of the eight steps in the TCA cycle, one of which involves Sdh, for specific metabolic uses.<sup>33</sup> In the glyoxylate pathway, isocitrate is converted to glyoxylate and sequentially converted to malate, thereby bypassing several transformations including the oxidation of succinate. Alternatively, isocitrate can also be directly converted to succinate. However, in this pathway, the succinate produced is often released for energy production and biosynthesis, suggesting metabolism and subsequent cellular function can persist without Sdh.

Based on this understanding of the TCA cycle, we postulated that we could rationalize the species-selectivity of promysalin on differences in metabolism which would become clear through microbiological growth assays in defined media. Toward this end, we first attempted, albeit unsuccessfully, to rescue growth of Pa through media supplementation of fumarate. These results were not surprising based on the dual modality of Sdh, as this enzyme not only converts succinate to fumarate but also facilitates electron transport. Although the supplementation assay would rescue the former deficiency, it would not address the latter. We next hypothesized that through purposefully selected feeding studies we could potentially override any inherent species-specific preferences in primary metabolism. To begin, we grew each strain (PA14, PAO1, PP KT2440, and PP RW10S1) in either TSB or M9 minimal media supplemented with either succinate or glucose. As expected, promysalin was active only against Pa and not Pp in TSB and M9 media supplemented with glucose as these carbon sources allowed the bacteria to utilize either the full TCA cycle or the shunt pathway in a fully aerobic process. Conversely, a clear zone of inhibition is present in both Pp strains (gentamicin shown as a control) as can be seen in Figure 5B, including the producing organism, demonstrating that promysalin is capable of inhibiting the growth of Pp in presumably nonenvironmental circumstances. While inhibition of the producing organism is surprising, it is not unprecedented as bacteria can develop modes of self-resistance to their own antibiotics. Toward this end, we sought to explain this finding by revisiting the isolation paper where the genome of the producing strain was fully sequenced. 10 In that report, no transporter or resistance genes were disclosed; however, the

gene cluster encoding the biosynthesis of the natural product is found immediately adjacent to the TCA genes and presumably under the control of the same promoter. This would allow the bacteria to modify its metabolism accordingly whenever antibiotic production was activated. Taken in sum, these results shed light on how promysalin can elicit is species-selectivity through the inhibition of Sdh.

#### DISCUSSION

We report herein a multidisciplinary approach to identify the biological target of the Pseudomonad secondary metabolite promysalin. Based on the narrow-spectrum activity of the natural product, we expected to either identify a target unique to Pa or a transporter specific to the natural product. Instead, we uncovered succinate dehydrogenase, an enzyme involved in primary metabolism, as the biological target; computational modeling, in vitro assays, and whole genome sequencing of resistant mutants further validated these findings. Previous studies have shown that other rhizosphere natural products, like siccanin, a fungal natural product, also target Sdh. This small molecule was "rediscovered" through an initial screen for Pa membrane inhibitors but was later shown to be species-selective preferentially targeting Pa, but not E. coli or Corynebacterium glutamicum.<sup>34</sup> When considering promysalin and siccanin, recent studies investigating the effect of growth conditions on essential functions of Pa confirm SdhABCD as essential, regardless of growth media. These findings complement the siccanin data, as SdhABCD has been found to be nonessential in corresponding E. coli investigations.<sup>35</sup> This difference in activity can be understood via the dual roles that Sdh serves both in metabolism by means of the TCA cycle and in respiration through the electron transport chain (ETC). While Pa is able, under specific conditions, to grow and survive via fermentation, respiration is almost solely responsible for ATP production (via oxidative phosphorylation following the ETC); consequently, unless in the proper environment, Pa requires the ETC to generate ATP and survive. 35,36 This facultative anaerobic behavior is a critical difference between Pa and Pp as Pp possesses a highly versatile aerobic metabolism, often favoring the Entner-Doudoroff pathway.<sup>37</sup> Furthermore, recent work by the Collins lab has demonstrated that metabolic flux in Pa greatly varies between growth conditions (i.e., carbon sources), and that by targeting specific enzymes within the TCA cycle, one can potentiate antibiotic activity. These findings may help to explain the differential activity between PAO1 and PA14, though they cannot fully rationalize the inactivity in Pp. 13 In a separate study looking at systems-level metabolic pathways, it has been postulated that Pp may be able to interchangeably utilize the glyoxylate shunt pathway in lieu of the TCA cycle without sacrificing overall growth.<sup>38</sup> Future work in our laboratory will seek to confirm these computational findings via transcriptomic studies.

Growth of Pa in sublethal concentrations of promysalin over a 24 day period led to the identification of a single, consistent mutation in SdhB, which was conserved across all replicates. This mutation, I206V, presumably results in a reduction of hydrophobic contacts with promysalin, reducing its affinity, while only having a minor effect on ubiquinone binding as demonstrated by its similar growth profile. In addition to the SdhB mutation, a portion of the resistant population also displayed the SCV phenotype, which WGS revealed to be a double mutant of both SdhB and YfiR. The abnormal morphology of the single colonies, containing the YfiR

mutation, is consistent with YfiR knockouts, which were first discovered in Pa CF sputum isolates. YfiR acts as the regulator in the YfiBNR system closely regulating YfiN, which functions as a diguanylate cyclase, producing c-di-GMP. In wild-type strains, YfiN is repressed by YfiR; however, in YfiR mutants, the derepression of YfiN leads to an increased production of c-di-GMP. Adaptations of this mutation increase the number of persister cells and also form more robust biofilms (Figure 4A). Presumably, the initial YfiR mutation in Pa arose in a similar manner, that is, from the sublethal treatment of antibiotic. It will be interesting to see if the mutation of YfiR is a common defense mechanism utilized by Pa to resist antibiotic treatment.

Taken together, we initially identified the target of a speciesselective antibiotic via proteomic studies. The success of these studies hinged on our previous analog findings thereby allowing for the chemical synthesis of a diazirine photoprobe which retained activity. Succinate dehydrogenase was identified using AfBPP and was further validated with in vitro assays, feeding studies, and whole genome sequencing of resistant mutants. Computational molecular docking was used to predict the putative binding pose within the ubiquinone pocket, and additionally provided insight into the basis for the observed I206V resistance mutation. Furthermore, we show that, under specific media conditions, the species-selective nature of promysalin is abolished to the extent that it is capable of inhibiting growth of its producing strain. Our findings add to the emerging discoveries focusing on the targeting of the TCA cycle both to potentiate existing antibiotics and also to develop narrow-spectrum therapies, which will undoubtedly find utility both in drug discovery and in deconvoluting multispecies microbiomes.

### ASSOCIATED CONTENT

## **S** Supporting Information

The Supporting Information is available free of charge on the ACS Publications website at DOI: 10.1021/jacs.7b11212.

Experimental details, synthesis details, NMR spectra (PDF)

#### AUTHOR INFORMATION

# **Corresponding Author**

\*wwuest@emory.edu

#### ORCID

Christian Fetzer: 0000-0001-5510-1544 John Karanicolas: 0000-0003-0300-726X Stephan A. Sieber: 0000-0002-9400-906X William M. Wuest: 0000-0002-5198-7744

#### Notes

The authors declare no competing financial interest.

## ACKNOWLEDGMENTS

This work was supported by the National Science Foundation CHE1755698(W.M.W.), the National Institute of General Medical Studies R35 GM119426 (W.M.W.), and Temple University. D.V.T. is supported by Grant EY028222 from the National Eye Institute. We thank Prof. Eric Brown (McMaster University), Prof. James Naismith (The University of St. Andrews), Prof. Louise Charkoudian (Haverford College), and Mr. Sean Rossiter (Temple University) for fruitful discussions, Materia, Inc. for olefin metathesis catalysts, Dr. Charles W.

Ross III, Director - Automated Synthesis and Characterization, of the University of Pennsylvania Chemistry Department Mass Spectrometry Facilities for mass spectral data, Dr. Charles DeBrosse for assistance with spectroscopy, and Profs. De Mot (KU-Leuven) and O'Toole (Dartmouth Medical School) for strains. We are grateful to OpenEye Scientific Software (Santa Fe, NM) for providing an academic license for the use of OMEGA, ROCS, and FastROCS. Computational resources were provided through National Science Foundation XSEDE allocation MCB130049.

#### REFERENCES

- (1) Fair, R. J.; Tor, Y. Perspect. Med. Chem. 2014, 6, 25.
- (2) Walsh, C. Nature 2000, 406, 775.
- (3) Maxson, T.; Mitchell, D. A. Tetrahedron 2016, 72, 3609.
- (4) Keohane, C. E.; Steele, A. D.; Wuest, W. M. Synlett 2015, 26,
- (5) Philippot, L.; Raaijmakers, J. M.; Lemanceau, P.; van der Putten, W. H. Nat. Rev. Microbiol. 2013, 11, 789.
- (6) Gellatly, S. L.; Hancock, R. E. W. Pathog. Dis. 2013, 67, 159.
- (7) Antibiotic Resistance Threats in the United States, 2013. https://www.cdc.gov/drugresistance/threat-report-2013/ (accessed March 27, 2017).
- (8) Vlassak, K.; Van Holm, L.; Duchateau, L.; Vanderleyden, J.; De Mot, R. *Plant Soil* 1992, 145, 51.
- (9) Herrmann, J.; Fayad, A. A.; Muller, R. Nat. Prod. Rep. 2017, 34, 135.
- (10) Li, W.; Estrada-de los Santos, P.; Matthijs, S.; Xie, G.; Busson, R.; Cornelis, P.; Rozenski, J.; De Mot, R. Chem. Biol. 2011, 18, 1320.
- (11) Steele, A. D.; Knouse, K. W.; Keohane, C. E.; Wuest, W. M. J. Am. Chem. Soc. 2015, 137, 7314.
- (12) Gorska, A.; Sloderbach, A.; Marszałł, M. P. Trends Pharmacol. Sci. 2014, 35, 442.
- (13) Meylan, S.; Porter, C. B. M.; Yang, J. H.; Belenky, P.; Gutierrez, A.; Lobritz, M. A.; Park, J.; Kim, S. H.; Moskowitz, S. M.; Collins, J. J. Cell Chem. Biol. 2017, 24, 195.
- (14) Braun, V.; Pramanik, A.; Gwinner, T.; Köberle, M.; Bohn, E. BioMetals 2009, 22, 3.
- (15) Wencewicz, T. A.; Miller, M. J. J. Med. Chem. 2013, 56, 4044.
- (16) Ji, C.; Juarez-Hernandez, R.; Miller, M. Future Med. Chem. 2012, 4. 297.
- (17) Butler, M. S.; Blaskovich, M. A. T.; Cooper, M. A. J. Antibiot. **2017**, 70, 3.
- (18) van Delden, C.; Page, M. G. P.; Köhler, T. Antimicrob. Agents Chemother. 2013, 57, 2095.
- (19) Moynié, L.; Luscher, A.; Rolo, D.; Pletzer, D.; Tortajada, A.; Weingart, H.; Braun, Y.; Page, M. G. P.; Naismith, J. H.; Köhler, T. *Antimicrob. Agents Chemother.* **2017**, *61*, e02531 PDB file: http://www.rcsb.org/pdb/explore.do?structureId=Sfp1.
- (20) Noinaj, N.; Guillier, M.; Barnard, T. J.; Buchanan, S. K. Annu. Rev. Microbiol. 2010, 64, 43.
- (21) Li, Z.; Hao, P.; Li, L.; Tan, C. Y. J.; Cheng, X.; Chen, G. Y. J.; Sze, S. K.; Shen, H.; Yao, S. Q. Angew. Chem., Int. Ed. 2013, 52, 8551.
- (22) Steele, A. D.; Keohane, C. E.; Knouse, K. W.; Rossiter, S. E.; Williams, S. J.; Wuest, W. M. J. Am. Chem. Soc. 2016, 138, 5833.
- (23) Boersema, P. J.; Raijmakers, R.; Lemeer, S.; Mohammed, S.; Heck, A. J. R. *Nat. Protoc.* **2009**, *4*, 484.
- (24) Cayman Chemical. MitoCheck Complex II Activity Assay Kit (700940).
- (25) Yankovskaya, V.; Horsefield, R.; Tornroth, S.; Luna-Chavez, C.; Miyoshi, H.; Leger, C.; Byrne, B.; Cecchini, G.; Iwata, S. *Science* **2003**, 299, 700.
- (26) Sierotzki, H.; Scalliet, G. Phytopathology 2013, 103, 880.
- (27) Shima, Y.; Ito, Y.; Hatabayashi, H.; Koma, A.; Yabe, K. Biosci., Biotechnol., Biochem. 2011, 75, 181.
- (28) Ito, Y.; Muraguchi, H.; Seshime, Y.; Oita, S.; Yanagi, S. O. *Mol. Genet. Genomics* **2004**, *272*, 328.

- (29) Li, S.; Li, T.; Xu, Y.; Zhang, Q.; Zhang, W.; Che, S.; Liu, R.; Wang, Y.; Bartlam, M. Sci. Rep. 2015, S, 16915.
- (30) Malone, J. G.; Jaeger, T.; Spangler, C.; Ritz, D.; Spang, A.; Arrieumerlou, C.; Kaever, V.; Landmann, R.; Jenal, U. *PLoS Pathog.* **2010**, *6*, e1000804.
- (31) Akram, M. Cell Biochem. Biophys. 2014, 68, 475.
- (32) Hederstedt, L.; Rutberg, L. Microbiol. Rev. 1981, 45, 542.
- (33) Kornberg, H. L. Biochem. J. 1966, 99, 1.
- (34) Mogi, T.; Kawakami, T.; Arai, H.; Igarashi, Y.; Matsushita, K.; Mori, M.; Shiomi, K.; Omura, S.; Harada, S.; Kita, K. *J. Biochem.* **2009**, 146, 383.
- (35) Lee, S. A.; Gallagher, L. A.; Thongdee, M.; Staudinger, B. J.; Lippman, S.; Singh, P. K.; Manoil, C. *Proc. Natl. Acad. Sci. U. S. A.* **2015**, *112*, 5189.
- (36) Wu, M.; Guina, T.; Brittnacher, M.; Nguyen, H.; Eng, J.; Miller, S. I. J. Bacteriol. **2005**, 187, 8185.
- (37) Chavarria, M.; Nikel, P. I.; Pérez-Pantoja, D.; de Lorenzo, V. Environ. Microbiol. 2013, 15, 1772.
- (38) Fahnoe, K. C.; Flanagan, M. E.; Gibson, G.; Shanmugasundaram, V.; Che, Y.; Tomaras, A. P. *PLoS One* **2012**, *7*, e51732.
- (39) Malone, J. C.; Jaeger, T.; Manfredi, P.; Dötsch, A.; Blanka, A.; Bos, R.; Cornelis, G. R.; Häussler, S.; Jenal, U. *PLoS Pathog.* **2012**, *8*, e1002760.